Improved results for the excited states of nitric oxide, including the *B*/*C* avoided crossing

Huancong Shi and Allan L. L. East[a)]
Department of Chemistry and Biochemistry, University of Regina, Regina, Saskatchewan S4S 0A2, Canada

(Received 12 June 2006; accepted 17 July 2006; published online 13 September 2006)

The potential energy surfaces of ten electronic states of nitric oxide (NO) have been reexamined computationally, with state energies calculated using *ab initio* multireference methods. Our wave function expansions of 10×10^6 configurations improve upon the results of de Vivie and Peyerimhoff [J. Chem. Phys. **89**, 3028 (1988)], who obtained excellent results from expansions of 16 000 configurations in 1988. We present results for the adiabatic properties r_e, B_e, T_e, and ω_e, demonstrating standard errors of 0.012 Å, 0.026 cm^{-1}, 620 cm^{-1}, and 41 cm^{-1}, respectively. Vertical excitation energies and oscillator strengths are also presented, as are potential energy surface curves, with special attention to the *B*/*C* avoided crossing. The technical issue of state-averaging effects is also discussed. © *2006 American Institute of Physics*.
[DOI: 10.1063/1.2336214]

I. INTRODUCTION

Time-resolved pump-probe spectroscopy experiments are generating renewed interest in excited-state potential energy surfaces (PESs), particularly at ground-state geometries and at geometries where state crossings and avoided crossings occur. For example, a popular system of study is the photodissociation of the dimer of nitric oxide, $(NO)_2 \rightarrow 2NO$,[1–13] and recent femtosecond time-resolved experiments at 6 eV pump energies have unraveled a particularly interesting electronic state evolution, from an initial valence charge-transfer (charge-resonance) state towards a ground ($X\,^2\Pi$) and excited Rydberg ($A\,^2\Sigma^+$) pair of monomers.[13] The electronic evolution is controlled by the PESs of the excited states. To assist in the spectral interpretation of 6 eV photodissociation of $(NO)_2$, we cataloged the numerous electronic states of the NO dimer[14] by relating them to well-known[15] states of the NO monomer, and participated in quantum chemistry calculations to elucidate the mechanism.[14]

However, at slightly higher energies, photodissociation of the dimer can produce NO fragments in a variety of excited states.[1,11] Such product distributions should depend quite heavily on the excited-state PESs of the intramonomer stretch modes of the dimer. We suspect that the PESs in this dimension may be similar to the PESs of the monomer itself, due to the almost perpendicular motions of intermonomer versus intramonomer stretch modes, and their moderately weak coupling due to the weak strength of the intermonomer bond in the ground state. Should this comparison be a good one, then the precise location of the $B\,^2\Pi/C\,^2\Pi$ avoided crossing of the monomer becomes relevant here, because it may control the *B* vs *C* product distributions of $(NO)_2$ photodissociation. Other state crossings also occur further down the dissociation channel. For these reasons we chose to revisit the PESs of the nitric oxide monomer.

A *tour de force* paper of *ab initio* excited-state PES results for NO was provided in 1988,[16] in the first of three papers by de Vivie and Peyerimhoff.[16–18] In Ref. 16, hereafter called "1988 results," they obtained very good results (e.g., roughly 1300 cm^{-1} accuracy in adiabatic T_e values) by employing configuration interaction (CI) with an energy-based configuration selection, using roughly 16 000 configurations for each state. The goal of the present paper is to present a smaller subset of improved results, relevant for modern experiments on the monomer and the dimer.

The paper starts with a technical discussion of the effects of state averaging on the orbital-optimization procedures. Then we present our new results for adiabatic properties (T_e, ω_e, r_e, and B_e) for several states, demonstrating the improvement over the 1988 results. This is followed by a specific presentation for the *B*/*C* avoided crossing and some vertical excitation results. Finally, a plot of our best estimate of the true PES curves is provided.

II. COMPUTATIONAL DETAILS

Calculations were performed with the MOLPRO 2002 code[19] in single-processor mode. The complete active space self-consistent field (CASSCF),[20,21] internally contracted multireference configuration interaction singles and doubles (MRCISD),[22–24] and Davidson-corrected internally contracted MRCISD+*Q* (Ref. 25) methods were applied. The N and O 1*s*-like core molecular orbitals were kept doubly occupied in all configurations, and the CASSCF(11, 12) active space consisted of a full-valence space plus the four Rydberg 3*s* and 3*p* orbitals (totaling $6a_1, 3b_1, 3b_2, 0a_2$ in C_{2v} symmetry).

The electronic configurations and states of NO monomer are well known. This paper concerns the doublet states, and

a)Electronic mail: allan.east@uregina.ca

TABLE I. Doublet electronic states of NO.

Valence configuration	Bond order	r_e (Å)[a]	Electronic states
$\sigma^2 n^2 n^2 \pi^4 \pi^{*1}$	2.5	1.15	$X\ ^2\Pi$
$\sigma^2 n^2 n^2 \pi^4 \mathrm{Ryd}^1$	3.0	1.06	$A\ ^2\Sigma^+$, $C\ ^2\Pi$, $D\ ^2\Sigma^+$
$\sigma^2 n^2 n^2 \pi^3 \pi^{*2}$	1.5	1.42	$B\ ^2\Pi$, $L\ ^2\Pi$, $L'\ ^2\Phi$, $4\ ^2\Pi$
$\sigma^2 n^2 n^1 \pi^4 \pi^{*2}$	2.0	~1.32	$B'\ ^2\Delta$, $G\ ^2\Sigma^-$, $I\ ^2\Sigma^+$

[a]Equilibrium bond lengths from experiment (see Table III).

they are summarized in Table I. Although the symmetry of the linear diatomic molecule belongs to the $C_{\infty v}$ point group, MOLPRO requires description of the states in C_{2v} symmetry. The correlations are $\Sigma^+ \rightarrow A_1$, $\Sigma^- \rightarrow A_2$, $\Pi \rightarrow \{B_1, B_2\}$, $\Delta \rightarrow \{A_1, A_2\}$, and $\Phi \rightarrow \{B_1, B_2\}$. The LQUANT flag is used to produce states of correct orbital angular momentum, which distinguishes between Σ and Δ states, and between Π and Φ states.

In state-averaged (SA) CASSCF calculations, the orbitals are optimized in a way that is optimal for the weighted-average energy of a group of states. The weighting was chosen to be equal for each state, rather than each configuration, e.g., the singly degenerate Σ states were doubly weighted while both configurations of the doubly degenerate Π, Δ, and Φ states were singly weighted.

In full-weight (FW) CASSCF calculations, the orbitals are optimized for one state only. In several cases, particularly states which are not the lowest state of a given symmetry, convergence was not achieved, and the FW result was obtained from weight extrapolation of SA results; e.g., if three runs applied weights of 50%, 60%, and 75% (respectively) to the state of interest, the FW result was obtained from parabolic extrapolation to 100% weighting. We tried this weight-extrapolation idea on some NO dimer states in 1998 with success.[26]

Two augmented correlation-consistent atomic-orbital basis sets are used: VTZ+R is the unmodified Dunning aug-cc-pVTZ basis set (overall contracted set $5s4p3d2f$),[27] and VTZ+2R is a modified version in which the diffuse s and p sets were replaced with two s and two p sets, built in an even-tempered way from the two most diffuse valence s and p functions (overall contracted set $6s5p3d2f$). The most significant effect of switching from VTZ+R to VTZ+2R was to lower the total energy of Rydberg states by 2000–4000 cm^{-1}. The effect upon the ground-state energy was negligible in FW runs ($<70\ \mathrm{cm}^{-1}$), but got as high as $+1500\ \mathrm{cm}^{-1}$ if the state was combined with Rydberg states in a SA run.

III. RESULTS AND DISCUSSION

A. Technical issue: State-averaged versus full-weight results

State averaging is one technique used to combat difficult CASSCF convergence cases for excited states. First we compare state-averaged PES results to full-weight ones, at a reduced level of theory (CASSCF/VTZ+R), to gauge the effects of state averaging. The set of states chosen for state

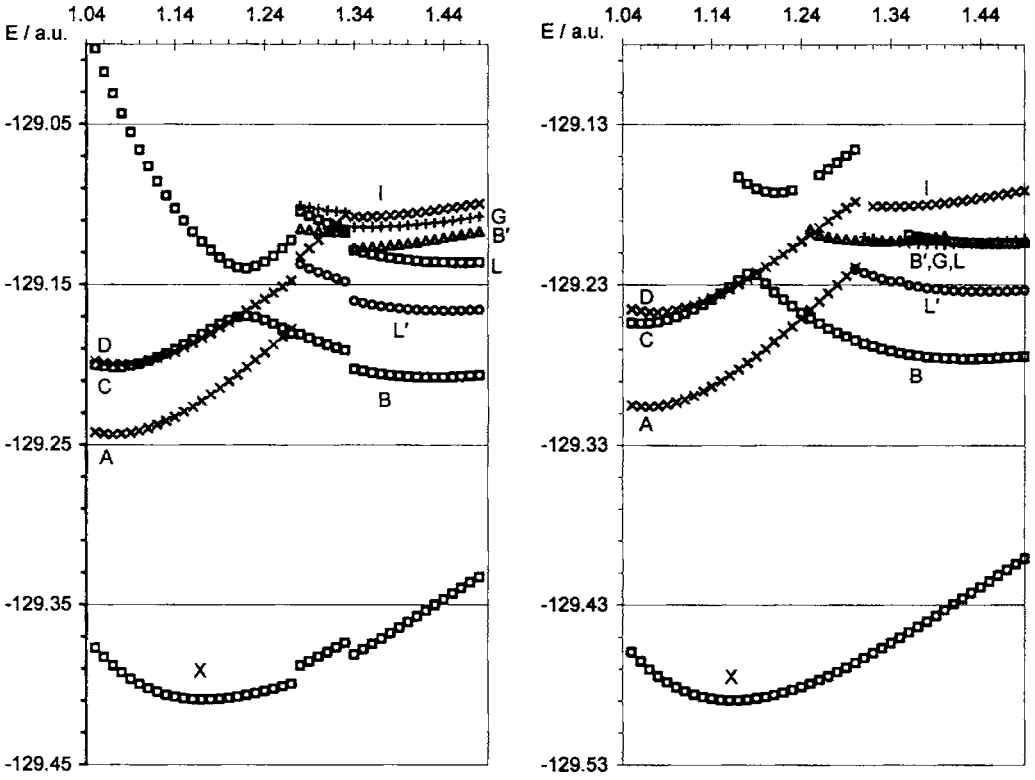

FIG. 1. CASSCF/VTZ+R PES plots vs R(N–O) (Å) comparing state-averaged (left) vs full-weight (right) results. (Left plot) Region I (1.05–1.27 Å): 5SA calculation ($XABCD$); region II (1.28–1.33 Å): 7SA calculation ($XABB'GLL'$); region III (1.34–1.48 A): 7SA calculation ($XBB'GILL'$). The states (not the configurations) were evenly weighted. (Right plot) Direct FW calculations in most cases, but weight extrapolation of SA data was used for the D state (with A:50/50, 70/30, 80/20), and for the $^2\Pi$ $\{C,B,L\}$ states, $2\ ^2\Pi$ (with X:50/50, 70/30, 80/20) and $3\ ^2\Pi$ (with $2\ ^2\Pi$ and X:60/20/20, 80/10/10, 90/5/5).

TABLE II. CASSCF/VTZ+R adiabatic results from both the SA and FW algorithms.

	SA			FW		
State	r_e (Å)	E (a.u.)	T_e (cm^{-1})	r_e (Å)	E (a.u.)	T_e (cm^{-1})
$X\,^2\Pi$	1.17	−129.409 481	⋯	1.16	−129.489 673	⋯
$A\,^2\Sigma^+$	1.07	−129.243 451	36 439	1.07	−129.305 926	40 328
$C\,^2\Pi$	1.07	−129.201 648	45 614	1.06	−129.254 209	51 678
$D\,^2\Sigma^+$	1.08	−129.199 844	46 010	1.08	−129.247 048	53 250
$B'\,^2\Delta$	~1.34	−129.127 081	61 980	1.33	−129.202 547	63 017
$G\,^2\Sigma^-$	1.36	−129.114 060	64 837	1.40	−129.204 680	62 549
$I\,^2\Sigma^+$	~1.34	−129.107 780	66 216	1.34	−129.181 090	67 726
$B\,^2\Pi$	1.43	−129.207 777	44 269	1.43	−129.276 162	46 860
$L\,^2\Pi$	1.46	−129.136 336	59 948	1.46	−129.204 275	62 638
$L'\,^2\Phi$	1.44	−129.166 237	53 386	1.44	−129.234 204	56 069

averaging was different for different bond-length regions, to allow algorithm convergence for a broad range of bond lengths (1.05–1.49 Å). The resulting PES curves appear in Fig. 1 (left). There are discontinuous jumps at 1.28 and 1.34 Å, due to the change in selection of states for the state averaging. Such discontinuous jumps were unavoidable with the SA algorithm, since the algorithm chooses the lowest-energy states within each symmetry block, and the lowest set at short bond lengths (mostly Rydberg states) is not the same as the set at larger bond lengths. For instance, the largest discontinuous jump (0.04 a.u.) was for the $A\,^2\Sigma(3s)$ state at 1.28 Å, due to the sudden arrival of many valence states into the state averaging, which decreased the importance of optimizing Rydberg orbitals. Interestingly, discontinuous jumps were not a problem for Polák and Fišer for the PES of four of these states, from MRCISD calculations based on four-state-averaged CASSCF calculations.[28] This comparison suggests that the smoothness of SA-based PES curves may be improved if (i) equal numbers of states are chosen for each geometry region and/or if (ii) MRCISD is used instead of CASSCF, which may serve to reduce the effect of differing orbital-optimization procedures by bringing the energies closer to full-CI results.

Full-weight calculations presented convergence difficulties for the second Σ state (D) and the second and third Π states (variously C, B, or L, depending on the geometry). To achieve convergence, weight extrapolation of SA data was performed, as indicated in the figure caption. The results appear in Fig. 1 (right). The weight-extrapolation procedure appears to work well, considering the smoothness of the resulting PES curves.

The effects of state averaging upon equilibrium bond lengths r_e and adiabatic excitation energies T_e are of particular interest. Table II presents these values from the SA and FW data of Fig. 1. The SA and FW values for r_e agree to 0.01 Å, except for the $G\,^2\Sigma^-$ state. For T_e values, SA results are generally smaller than FW results, by 4000–7000 cm^{-1} for Rydberg states and by 1000–2700 cm^{-1} for valence states, except the $G\,^2\Sigma^-$ state for which the SA value is 2300 cm^{-1} higher than the FW value. Since FW results should always produce a better wave function for a given state than SA results, we conclude here that state averaging produces "more approximate" T_e values.

TABLE III. Calculated results for r_e (Å) from FW calculations using VTZ+2R basis set (VTZ+R was used for the B and L states).

State	MRCISD	MRCISD+Q	1988[a]	Expt.[b]
$I\,^2\Sigma^+$	1.319	1.319	⋯	⋯
$G\,^2\Sigma^-$	1.360	1.359	1.354	1.343
$L\,^2\Pi$	1.448	1.450	1.487	1.399[c]
$L'\,^2\Phi$	1.438	1.439	1.422	1.422[d]
$B'\,^2\Delta$	1.314	1.314	1.310	1.302
$D\,^2\Sigma^+$	1.073	1.074	1.086	1.061
$C\,^2\Pi$	1.067	1.068	1.066	1.062
$B\,^2\Pi$	1.424	1.427	1.428	1.416
$A\,^2\Sigma^+$	1.070	1.071	1.063	1.063
$X\,^2\Pi$	1.158	1.159	1.159	1.151
Std. err.	*0.011*	*0.012*	*0.011*	

[a]1988 MRCI results of de Vivie and Peyerimhoff (Ref. 16).
[b]Huber and Herzberg (Ref. 29).
[c]Dressler and Miescher (Ref. 31); value not included in standard error calculation.
[d]Taherian *et al.* (Ref. 30).

TABLE IV. Calculated results for B_e (cm^{-1}) from FW calculations using VTZ+2R basis set (VTR+R was used for the B and L states).

State	MRCISD	MRCISD+Q	1988[a]	Expt.[b]
$I\,^2\Sigma^+$	1.299	1.298	⋯	⋯
$G\,^2\Sigma^-$	1.221	1.223	1.231	1.252
$L\,^2\Pi$	1.076	1.074	1.021	1.154[c]
$L'\,^2\Phi$	1.092	1.090	1.116	1.117
$B'\,^2\Delta$	1.307	1.307	1.315	1.332
$D\,^2\Sigma^+$	1.962	1.959	1.911	2.006
$C\,^2\Pi$	1.984	1.980	1.984	2.002
$B\,^2\Pi$	1.113	1.109	1.106	1.126
$A\,^2\Sigma^+$	1.973	1.969	1.998	1.998
$X\,^2\Pi$	1.682	1.681	1.678	1.704
Std. err.	*0.025*	*0.026*	*0.034*	

[a]1988 MRCI results of de Vivie and Peyerimhoff (Ref. 16).
[b]Rederived (=$2.2577/R_e^2$) from the experimental bond lengths of Table III to avoid confusion with spin-orbit components of $^2\Pi$ states (which may have affected the values reported in Ref. 16).
[c]Value not included in standard error calculation.

TABLE V. Calculated results for T_e (cm^{-1}) from FW calculations using VTZ+2R basis set (VTZ+R was used for the B and L states).

State	MRCISD	MRCISD+Q	1988[a]	Expt.[b]
$I\,^2\Sigma^+$	66 374	65 691	⋯	⋯
$G\,^2\Sigma^-$	62 708	62 334	61 933	62 913
$L\,^2\Pi$	61 497	61 126	60 007	61 563.0[c]
$L'\,^2\Phi$	53 488	52 975	52 281	53 675.5[d]
$B'\,^2\Delta$	60 482	59 911	60 596	60 364.2
$D\,^2\Sigma^+$	52 050	52 492	52 080	53 084.7
$C\,^2\Pi$	51 201	51 808	51 864	52 126
$B\,^2\Pi$	45 236	44 803	43 414	45 913.6
$A\,^2\Sigma^+$	42 889	43 558	45 137	43 965.7
$X\,^2\Pi$	0	0	0	0
Std. err.	*675*	*620*	*1327*	

[a]1988 MRCI results of de Vivie and Peyerimhoff (Ref. 16).
[b]Huber and Herzberg (Ref. 29); the zero of energy is the lowest spin-orbit component of the ground state, and hence these T_e values include a +61 cm^{-1} spin-orbit shift that is not included in the quantum chemistry calculations.
[c]Dressler and Miescher (Ref. 31).
[d]Taherian *et al.* (Ref. 30).

TABLE VI. Calculated results for ω_e (cm^{-1}) from FW calculations using VTZ+2R basis set (VTZ+R was used for the B and L states).

State	MRCISD	MRCISD+Q	1988[a]	Expt.[b]
$I\,^2\Sigma^+$	1073	1059	⋯	⋯
$G\,^2\Sigma^-$	1057	1050	1069	1085.5
$L\,^2\Pi$	959	953	892	974.6[c]
$L'\,^2\Phi$	976	976	920	1000.0[d]
$B'\,^2\Delta$	1201	1197	1167	1217.4
$D\,^2\Sigma^+$	2322	2323	2413	2323.9
$C\,^2\Pi$	2332	2328	2475	2395.0
$B\,^2\Pi$	1093	1108	1043	1037.2
$A\,^2\Sigma^+$	2345	2344	2219	2374.3
$X\,^2\Pi$	1864	1862	1836	1904.2
Std. err.	*36*	*41*	*81*	

[a]1988 MRCI results of de Vivie and Peyerimhoff (Ref. 16).
[b]Huber and Herzberg (Ref. 29).
[c]Dressler and Miescher (Ref. 31).
[d]Taherian *et al.* (Ref. 30).

B. Updated computational results for adiabatic properties

Our best results for adiabatic properties employed MRCISD+Q/VTZ+2R, based on full-weight CASSCF calculations and no other restrictions, and employed almost 10×10^6 configurations for each state. The results appear in Tables III–VI.

Table III focuses on the equilibrium bond lengths r_e of each state. All three sets of CI-based computed values are seen to give bond lengths that are generally ~0.01 Å too long. Table IV focuses on the equilibrium rotational constants B_e, inversely related to the square of r_e. The standard errors for B_e suggest an improvement over the 1988 values, unlike the data for r_e, but this is due only to the D state bond-length error in 1988 which is accentuated in the B_e data.

Table V focuses on the adiabatic T_e energies of each state. Here the improvement over the 1988 values is clear. Not only is the standard error smaller, for both the modern MRCISD and MRCISD+Q procedures, but the errors are more consistent, as shown more clearly in Fig. 2. The Davidson correction further ensured this consistency between Rydberg (A, C, and D) and valence states, which MRCISD did not provide. This improved consistency also improved state ordering, as the 1988 values gave an incorrect ordering of the $B\,^2\Pi$ and $A\,^2\Sigma^+$ states. We did have some difficulties with the C/D state ordering in CASSCF SA runs, although FW runs and MRCISD corrections cured these problems. (In our CASSCF SA runs, the inclusion of $B'\,^2\Delta$ or $L'\,^2\Phi$ caused an incorrect C/D state ordering, and hence neither of these states were included in the SA calculations at small bond lengths for Fig. 1.)

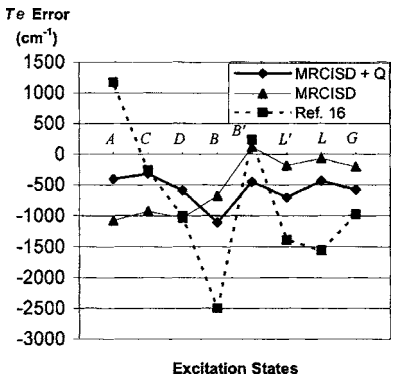

FIG. 2. Errors in the computed T_e values of Table V relative to experiment. Note the improved size and consistency of errors with the MRCISD+Q results.

Table VI focuses on the harmonic frequencies ω_e of each state. As with the T_e values, the computed ω_e values are improvements over the 1988 values, demonstrating ~40 cm^{-1} accuracy. Note that our results do not demonstrate the experimentally observed 50–70 cm^{-1} lowering of the frequency of the D Rydberg state, relative to the A and C states. The existing hypothesis is that the D ($3p_z$) Rydberg state is affected by orbital and state repulsion with the quite higher antibonding (σ^*) valence state,[32] due to strong orbital overlap.[33] Such effects should have been accessible by our calculation, since both these orbitals are contained in our active space. This curiosity must await even more accurate calculations.

The absence of experimental data for the $I\,^2\Sigma^+$ state could be due to the $A\,^2\Sigma^+/I\,^2\Sigma^+$ avoided crossing, which occurs quite near the I state diabatic minimum.[28]

C. The B/C avoided crossing

The $B\,^2\Pi/C\,^2\Pi$ avoided crossing results in an adiabatic double-well lower state which is a Rydberg state (C) at small bond lengths and a valence state (B) at large bond lengths. It should be of particular interest in photochemical experiments, because it occurs at a bond length rather near that of the ground state. We were interested in locating it more accurately.

We attempted FW-based results for this avoided crossing, but the weight-extrapolation trick failed here because the data could not be extrapolated: a smooth variation of weights

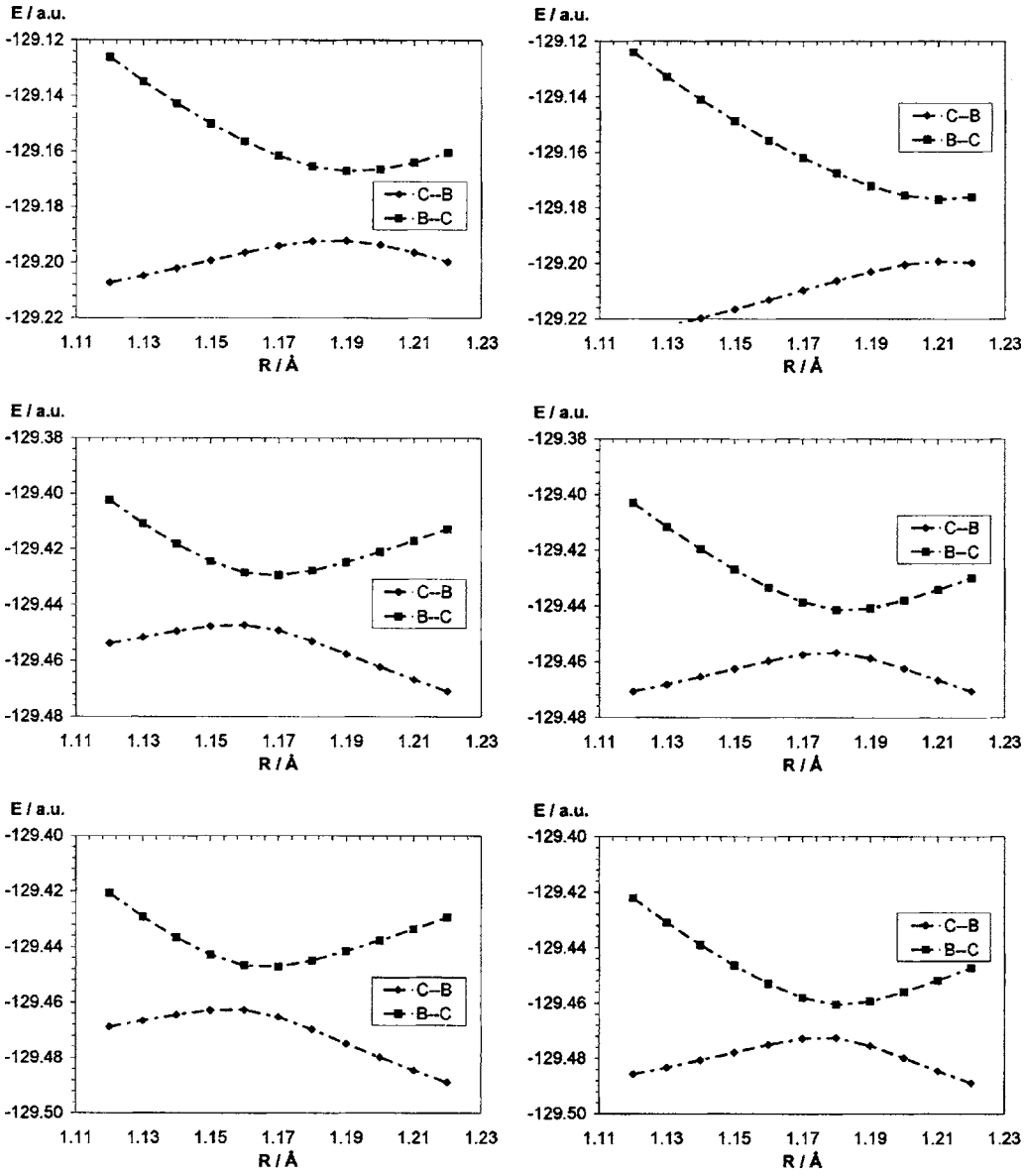

FIG. 3. Computed results for the *B*-*C* avoided crossing of NO monomer using (from top to bottom rows) CASSCF, MRCISD, and MRCISD+*Q* methods, and (from left to right) using VTZ+R and VTZ+2R basis sets. All are from state-averaged calculations (*X*/*B*/*C*/*L*, evenly weighted). The bottom right plot should be deemed the most accurate.

failed to maintain the identity of the states as 50/50 mixtures of the two diabatic states. Hence, we can only provide data based on state-averaged orbitals. Figure 3 presents our computed data for this avoided crossing, at six different combined levels of theory. Extra diffuse functions (moving from the left plots to the right plots) preferentially lower the diabatic Rydberg *C* state curve, forcing the crossing to the right. Dynamic correlation (moving from the top to bottom plots) preferentially lowers the diabatic valence *B* state curve, forcing the crossing to the left.

The best result in the figure (MRCISD+*Q*/VTZ+2R) places the avoided crossing at 1.18 Å, with an energy gap of 2634 cm^{-1} between the adiabatic states, and the center of the gap at an adiabatic energy of 57 623 cm^{-1}. The Davidson correction (*Q*) did not affect the location of the avoided crossing, although it did reduce the gap by roughly 22%. Table VII compares our computed values to literature ones for the *B*/*C* avoided crossing location and gap. Note that our fully *ab initio* calculation results in a crossing almost exactly where Gallusser and Dressler located it (1.183 Å, 57 350 cm^{-1} from their Fig. 1) from empirical fitting of vibronic data.[34]

TABLE VII. Properties of the $B\,^2\Pi/C\,^2\Pi$ avoided crossing.

Source	Bond length (Å)	Adiabatic energy center (cm^{-1})	Adiabatic energy gap (cm^{-1})
MRCISD/VTZ+2R	1.18	57 626	3365
MRCISD+*Q*/VTZ+2R	1.18	57 623	2634
de Vivie-Riedle *et al.*[a]	1.17	57 800	3230
Hiyama and Child[b]	1.25	60 000	···
Empirical fitting[c]	1.18	57 350	···

[a]Reference 18, except the energy center which is from Ref. 16.
[b]Reference 35.
[c]Reference 34.

TABLE VIII. Vertical excitation energies ΔE, transition dipole moments μ_{ij}, and oscillator strengths f_{ij} from MRCISD/VTZ+2R calculations [calculations based on 2SA CASSCF calculations (ground and target states), except the $X-D$ and $X-B$ calculations which were based on 3SA CASSCF calculations (the middle state being A and C in the respective calculations)].

			f_{ij}		
Transition	ΔE (cm^{-1})	μ_{ij}(a.u.)	Ours[a]	Expt.	$T1$[b]
$X-A\ ^2\Sigma^+$	46 532	−0.0895	0.001	0.0022[c]	0.007
$X-C\ ^2\Pi$	54 349	0.2749	0.012	0.0122[d]	0.004
$X-D\ ^2\Sigma^+$	54 550	0.2085	0.007	0.0108[d]	0.007
$X-B\ ^2\Pi$	61 071	−0.0231	0.000	0.0036[d]	0.000
$X-B'\ ^2\Delta$	66 070	−0.1584	0.005	···	0.009
$X-G\ ^2\Sigma^-$	66 242	−0.1572	0.005	···	···
$X-L'\ ^2\Phi$	69 215		Zero (forbidden)		

[a]From the formula $f=(3.037\times10^{-6}\ \text{cm})\cdot\bar{\nu}(\text{cm}^{-1})\cdot\langle\mu(\text{a.u.})\rangle^2$.
[b]Based on μ_{ij} values from Tables 4 and 6 of de Vivie and Peyerimhoff (Ref. 16) and ΔE from this table.
[c]From summing measured vibronic line-by-line data in Table I of Ref. 36.
[d]From summing measured vibronic line-by-line data in Table IV of Ref. 37.

D. Vertical excitation data

Table VIII presents vertical excitation energies and intensities (oscillator strengths or f values) for several electronic states. The calculations were based on 2SA or 3SA calculations in order to have a common set of orbitals for both ground and excited states, which simplifies the computation of the transition dipole moment.

The oscillator strengths are in better agreement with experiment[36,37] than the 1988 results. The ΔE values are expected to correspond to the maximum intensities of the individual electronic bands, although many of these bands are broad and overlap. The bands predicted to be centered near 66 000 cm^{-1}, due to the B' and G states, can be seen in the spectra of Lagerqvist and Miescher[38] as sets of three vibronic bands clustered at 64 500, 65 500, and 66 500 cm^{-1} (the $v'=4,5,6$ levels of B' and the $v'=2,3,4$ levels of G). The predicted centers for the Rydberg A, C, and D bands (experimentally called the γ, δ, and ε bands) are in very good agreement with the coarse experimental values of 5.9, 6.9, and 7.0 eV we discern from Fig. 2 of Zhu *et al.*[36]

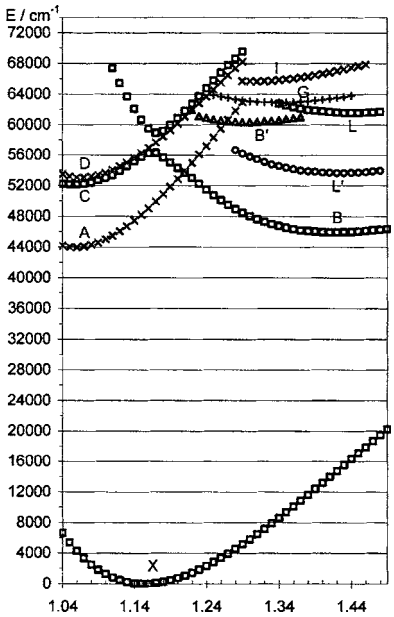

FIG. 4. Our best prediction of the true PES curves vs R(N–O) (Å), based on Fig. 1(b) and the B/C avoided crossing from MRCISD+Q/VTZ+2R, but shifted to fit experimental r_e and T_e values.

E. Final PES plot

Finally, we present in Fig. 4 our best prediction of the nonrelativistic (i.e., no spin-orbit splittings) PES curves. These data are also available in tabular format in the supplementary material (EPAPS),[39] for use in other applications.

IV. SUMMARY

The potential energy surfaces of ten electronic states of nitric oxide (NO) have been reexamined computationally, with state energies calculated using various CASSCF and MRCISD approaches. Our best results, from MRCISD +Q/VTZ+2R calculations, can reproduce experimental values for r_e, B_e, T_e, and ω_e, to within standard errors of 0.012 Å, 0.026 cm^{-1}, 620 cm^{-1}, and 41 cm^{-1}, respectively. Vertical excitation energies and oscillator strengths are also in very good agreement with experiment. The B/C avoided crossing is found to occur at R(N–O)=1.18 Å and centered at an adiabatic energy of 57 623 cm^{-1}, with an energy gap of 2634 cm^{-1}. Our best set of PES curves is presented, for use in future applications.

ACKNOWLEDGMENTS

Calculations were performed on a Parallel Quantum Solutions (USA) computer, obtained with the assistance of the Canada Foundation for Innovation (Canada) and managed by the Laboratory for Computational Discovery (University of Regina). NSERC (Canada) is thanked for an operating grant.

[1] O. Kajimoto, K. Honma, and T. Kobayashi, J. Phys. Chem. **89**, 2725 (1985).
[2] Y. Naitoh, Y. Fijumura, O. Kajimoto, and K. Honma, Chem. Phys. Lett. **190**, 135 (1992).
[3] Y. Naitoh, Y. Fujimura, K. Honma, and O. Kajimoto, Chem. Phys. Lett. **205**, 423 (1993).
[4] Y. Naitoh, Y. Fujimura, K. Honma, and O. Kajimoto, J. Phys. Chem. **99**,

13652 (1995).
[5] V. Blanchet and A. Stolow, J. Chem. Phys. **108**, 4371 (1998).
[6] M. Tsubouchi, C. A. de Lange, and T. Suzuki, J. Chem. Phys. **119**, 11728 (2003).
[7] M. Tsubouchi and T. Suzuki, Chem. Phys. Lett. **382**, 418 (2003).
[8] A. V. Demyanenko, A. B. Potter, V. Dribinski, and H. Reisler, J. Chem. Phys. **117**, 2568 (2002).
[9] A. B. Potter, V. Dribinski, A. V. Demyanenko, and H. Reisler, J. Chem. Phys. **119**, 7197 (2003).
[10] V. Dribinski, A. B. Potter, I. Fedorov, and H. Reisler, Chem. Phys. Lett. **385**, 233 (2004).
[11] V. Dribinski, A. B. Potter, I. Fedorov, and H. Reisler, J. Chem. Phys. **121**, 12353 (2004).
[12] A. B. Potter, J. Wei, and H. Reisler, J. Phys. Chem. B **109**, 8407 (2005).
[13] O. Geßner, A. M. D. Lee, J. P. Shaffer *et al.*, Science **311**, 219 (2006).
[14] S. V. Levchenko, H. Reisler, A. I. Krylov, O. Geßner, A. Stolow, H. Shi, and A. L. L. East, J. Chem. Phys. (to be published).
[15] E. Miescher and K. P. Huber, in *Spectroscopy*, International Review of Science, Physical Chemistry, Series 2, edited by D. A. Ramsay (Butterworths, London, 1976), Vol. 3.
[16] R. de Vivie and S. D. Peyerimhoff, J. Chem. Phys. **89**, 3028 (1988).
[17] R. de Vivie and S. D. Peyerimhoff, J. Chem. Phys. **90**, 3660 (1989).
[18] R. de Vivie-Riedle, M. C. van Hemert, and S. D. Peyerimhoff, J. Chem. Phys. **92**, 3613 (1990).
[19] H.-J. Werner, P. J. Knowles, M. Schütz *et al.*, MOLPRO, a package of *ab initio* programs.
[20] H.-J. Werner and P. J. Knowles, J. Chem. Phys. **82**, 5053 (1985).
[21] P. J. Knowles and H.-J. Werner, Chem. Phys. Lett. **115**, 259 (1985).
[22] H.-J. Werner and P. J. Knowles, J. Chem. Phys. **89**, 5803 (1988).
[23] P. J. Knowles and H.-J. Werner, Chem. Phys. Lett. **145**, 514 (1988).
[24] P. J. Knowles and H.-J. Werner, Theor. Chim. Acta **84**, 95 (1992).
[25] S. R. Langhoff and E. R. Davidson, Int. J. Quantum Chem. **8**, 61 (1974).
[26] A. L. L. East, J. Chem. Phys. **109**, 2185 (1998).
[27] R. A. Kendall, T. H. Dunning Jr., and R. J. Harrison, J. Chem. Phys. **96**, 6796 (1992).
[28] R. Polák and J. Fišer, Chem. Phys. Lett. **377**, 564 (2003).
[29] K. P. Huber and G. Herzberg, *Constants of Diatomic Molecules*, Molecular Spectra and Molecular Structure IV (Van Nostrand, New York, 1979).
[30] M. R. Taherian, P. C. Cosby, and T. G. Slanger, J. Chem. Phys. **83**, 3878 (1985).
[31] K. Dressler and E. Miescher, J. Chem. Phys. **75**, 4310 (1981).
[32] E. Miescher, Can. J. Phys. **54**, 2074 (1976).
[33] F. Ackermann, H. Lefebvre-Brion, and A. L. Roche, Can. J. Phys. **50**, 692 (1972).
[34] R. Gallusser and K. Dressler, J. Chem. Phys. **76**, 4311 (1982).
[35] M. Hiyama and M. S. Child, J. Phys. B **35**, 1337 (2002).
[36] L. F. Zhu, Z. P. Zhong, Z. S. Yuan, W. H. Zhang, X. J. Liu, X. M. Jiang, K. Z. Xu, and J. M. Li, Chin. Phys. **11**, 1149 (2002).
[37] K. Yoshino, A. P. Thorne, J. E. Murray, A. S.-C. Cheung, A. L. Wong, and T. Imajo, J. Chem. Phys. **124**, 054323 (2006).
[38] A. Lagerqvist and E. Miescher, Can. J. Phys. **44**, 1525 (1966).
[39] See EPAPS Document No. E-JCPSA6-125-304633 for an ascii file of the state energies plotted in Fig. 4. This document can be reached via a direct link in the online article's HTML reference section or via the EPAPS homepage (http://www.aip.org/pubservs/epaps.html).